Atmospheric
Chemistry
and Physics
Discussions

Open Access

EGU

1 **Aerosol Characteristics in the Entrainment Interface Layer In Relation to the Marine**
2 **Boundary Layer and Free Troposphere**
3
4 Hossein Dadashazar[1], Rachel A. Braun[1], Ewan Crosbie[2,3,] Patrick Y. Chuang[4], Roy K. Woods[5],
5 Haflidi H. Jonsson[5], Armin Sorooshian[1,6]
6
7
8 [1]Department of Chemical and Environmental Engineering, University of Arizona, Tucson, AZ,
9 USA
10 [2]Science Systems and Applications, Inc., Hampton, VA, USA
11 [3]NASA Langley Research Center, Hampton, VA, USA
12 [4]Earth and Planetary Sciences, University of California-Santa Cruz, Santa Cruz, CA, USA
13 [5]Naval Postgraduate School, Monterey, CA, USA
14 [6]Department of Hydrology and Atmospheric Sciences, University of Arizona, Tucson, AZ, USA
15
16
17 *Correspondence to:* Armin Sorooshian (armin@email.arizona.edu)

Atmospheric
Chemistry
and Physics
Discussions

Open Access

18 **Abstract.** This study uses airborne data from two field campaigns off the California coast to
19 characterize aerosol size distribution characteristics in the entrainment interface layer (EIL), a
20 thin and turbulent layer above marine stratocumulus cloud tops, that separates the stratocumulus-
21 topped boundary layer (STBL) from the free troposphere (FT). The vertical bounds of the EIL
22 are defined in this work based on considerations of buoyancy and turbulence using
23 thermodynamic and dynamic data. Aerosol number concentrations are examined from three
24 different probes with varying particle diameter (D_p) ranges: > 3 nm, > 10 nm, $0.11 - 3.4$ µm.
25 Relative to the EIL and FT layers, the sub-cloud (SUB) layer exhibited lower aerosol number
26 concentrations and higher surface area concentrations. High particle number concentrations
27 between 3 and 10 nm in the EIL is indicative of enhanced nucleation, assisted by high actinic
28 fluxes, cool and moist air, and much lower surface area concentrations than the STBL. Slopes of
29 number concentration versus altitude in the EIL were correlated with the particle number
30 concentration difference between the SUB and lower FT layers. The EIL aerosol size distribution
31 was influenced by varying degrees from STBL aerosol versus subsiding FT aerosol depending
32 on the case examined. These results emphasize the important role of the EIL in influencing
33 nucleation and aerosol-cloud-climate interactions.

Atmospheric
Chemistry
and Physics
Discussions

1. Introduction

Stratocumulus clouds are extensively studied because they are both the dominant cloud type by global area (Warren et al., 1986), covering approximately a fifth of the planet's surface area on an annual basis (Wood, 2012), and they play an important role in the planet's energy balance due to their impact on planetary albedo. The layer separating the stratocumulus-topped boundary layer (STBL) from the free troposphere (FT) aloft is usually tens of meters in vertical extent and referred to as the entrainment interface layer (EIL) (Caughey et al., 1982; Nicholls and Turton, 1986; Wang and Albrecht, 1994; Lenschow et al., 2000). This layer exhibits strong gradients in thermodynamic and dynamic properties. Although numerous airborne and modeling studies have attempted to increase our understanding about the thermodynamic and dynamic nature of the EIL (e.g., Caughey et al., 1982; Moeng et al,. 2005; Haman et al,. 2007; Wang et al,. 2008; Carman et al., 2012; Katzwinkel et al,. 2012; Gerber et al,. 2013; Malinowski et al,. 2013; Plante et al,. 2016), aerosol characteristics in this thin layer have not been studied in detail.

The nature of the aerosol layer immediately above cloud top is important to understand because particles impact cloud microphysics and also because clouds vertically redistribute particles, remove them via droplet coalescence, and transform their properties through aqueous reactions. A modeling study showed that aerosol entrainment from the FT can contribute up to between 69-89% of particle number concentrations in the marine boundary layer (Katoshevski et al., 1999), and field measurements have confirmed the importance of entrainment in shaping the marine boundary layer aerosol budget (e.g., Clarke et al., 1998). The effects of above-cloud aerosol particles on clouds depend on the physicochemical properties of particles, their vertical distance from cloud top, and the dynamic and thermodynamic conditions around cloud top. Particles closest to the cloud top can entrain into the cloud and change the number concentration and size distribution of droplets (Costantino and Breón, 2010). On the other hand, an aerosol layer more detached from the cloud top and higher aloft can potentially alter the thermodynamic and dynamic structure of the layer below it, such as with absorbing smoke layers that can lead to stabilization and weaker cloud top long wave radiative cooling. This could in turn reduce cloudiness and cloud radiative forcing (Yamaguchi et al., 2015).

The goal of this study is to examine vertically-resolved aircraft data in the marine atmosphere off the California coast to characterize aerosol characteristics as a function of altitude, with a focus on the EIL. The results provide insight into the degree of similarity between the aerosol size distribution in the EIL relative to the STBL and FT. The results motivate additional attention to the EIL in terms of acting as an intermediate layer between the STBL and FT, in which there is some combination of cloud-processed aerosol and FT aerosol, in addition to new particle formation.

2. Experimental Methods

Aircraft data from the Center for Interdisciplinary Remotely-Piloted Aircraft Studies (CIRPAS) Twin Otter are analyzed from the Nucleation in California Experiment (NiCE, 2013) and the Fog and Stratocumulus Evolution Experiment (FASE, 2016), both of which took place between July and August. The flights examined here typically lasted four hours and included vertical characterization of marine aerosol ranging from near the ocean surface (~ 50 m ASL) up to 2 km in altitude.

Navigational, dynamic, and thermodynamic data were obtained from standard instruments described in a number of previous studies (e.g., Crosbie et al., 2016; Wang et al., 2016; Dadashazar et al., 2017). Aerosol particle concentrations were measured using multiple condensation particle

80   counters (CPCs; TSI Inc.), specifically the CPC 3010 (particle diameter, $D_P > 10$ nm) and ultrafine
81   CPC (UFCPC) 3025 ($D_P > 3$ nm). The CPCs sampled downstream of a forward facing sub-
82   isokinetic inlet, which samples aerosol below 3.5 µm diameter with 100% efficiency (Hegg et al.,
83   2005). Aerosol size distributions were obtained with a Passive Cavity Aerosol Spectrometer Probe
84   (PCASP; $D_P \sim 0.11 – 3.4$ µm; Particle Measuring Systems (PMS), Inc., modified by Droplet
85   Measurement Technologies, Inc.). Data from the Forward Scattering Spectrometer Probe (FSSP;
86     $D_P \sim 1.6 – 45$ µm; PMS, Inc., modified by Droplet Measurement Technologies, Inc.) were
87   additionally used to quantify aerosol surface area concentrations for particle diameters exceeding
88   the PCASP upper size limit. Vertically-resolved droplet size distributions from the Cloud Imaging
89   Probe (CIP; D_P; 25–1550 µm) were used to estimate columnar-mean drizzle rates in clouds
90   according to documented relationships between drop size and fall velocity (e.g., Chen et al., 2012;
91   Feingold et al., 2013; Dadashazar et al., 2017).
92   The PVM-100 probe (Gerber et al., 1994) provided measurements of liquid water content
93   (LWC). A threshold LWC value of 0.02 g m^{-3} has been used extensively in the study region to
94   identify the presence of clouds (Prabhakar et al., 2014), which was important during soundings
95   to quantify cloud base and top heights. The presented analysis was conducted for cases when the
96   cloud layer was coupled to the surface layer rather than also considering decoupled clouds. We
97   follow the methods employed in Wang et al. (2016) to distinguish between the two types of
98   clouds based on discontinuities in thermodynamic variables from vertical sounding data.
99

100   **3. Results and Discussion**
101   **3.1 Layer Definitions**
102   A total of 17 spiral soundings were analyzed from FASE and NiCE, with their locations
103   shown in Figure 1. The ranges of cloud base heights and tops were 129-403 m and 375-729 m,
104   respectively, for these soundings. Three vertical layers were defined with respect to the cloud
105   layer including the sub-cloud (SUB) layer, the entrainment interface layer (EIL), and the FT. The
106   vertical bounds of the EIL are defined based on considerations of buoyancy and turbulence,
107   similar to past studies (Carman et al., 2012). An example from FASE Research Flight 7 (F07) on
108   1 August 2016 illustrates the criteria used to determine the vertical boundaries of the EIL, STBL,
109   and FT (Figure 2). While some studies extend the EIL into the cloud layer (Malinowski et al.,
110   2013; Plante et al., 2016), this work defines the base of the EIL at cloud top (i.e., uppermost
111   height where LWC ≥ 0.02 g m^{-3}) for practical reasons since aerosol data from the PCASP and
112   CPCs are not meaningful in the cloud layer. The top of the EIL is not as well-defined as its base
113   due to weaker vertical gradients of dynamic and thermodynamic properties relaxing to FT values
114   over tens of meters at times (Wood, 2012). A method similar to that of Malinowski et al. (2013)
115   is applied, where the top of the EIL is taken to be the highest point where turbulent kinetic
116   energy (TKE) and the variance of potential temperature (θ) simultaneously exceed 0.1 m^2 s^{-2} and
117   10% of maximum variance, respectively. This location is identified based on the smoothed
118   moving variance and average of 75 points of 10 Hz data used to calculate both the θ variance and
119   TKE for spiral soundings. Considering an ascent rate of ~1.5 m s^{-1}, 75 points corresponds to a
120   vertical distance of ~10 m. Based on the aforementioned criteria, the average (± standard
121   deviation) EIL thickness was 30 ± 15 m, with a minimum of 10 m and a maximum of 70 m
122   (Table 1).
123   The FT base is considered to be at the EIL top, while the STBL top marks the EIL base.
124   The FT layer extends up to 400 m above the EIL top for most cases except for five spirals that
125   only reached ~100 m above the EIL top (i.e., F10-1, F12-2, F14-1, F14-2, F16). In order to have

Atmospheric
Chemistry
and Physics
Discussions

126   a more detailed analysis, the FT is further stratified into 100 m thick layers for the 12 spirals that
127   afforded such data: FT1 = first 100 m increment above EIL top, FT2 = the 100 m increment
128   above FT1, and so forth.
129
130   **3.2 Cumulative Vertical Profiles**
131   Table 1 compares particle concentration measurements from the PCASP and CPCs
132   between the FT, EIL, and SUB layers. CPC concentrations were highest in the EIL for eight of
133   the 17 soundings, with the remaining nine cases exhibiting peak values in the FT. With
134   ascending altitude, average CPC concentrations were as follows: 465 ± 282 cm^{-3} (SUB), $1052 \pm$
135   390 cm^{-3} (EIL), 1036 ± 612 cm^{-3} (FT). When considering UFCPC data (i.e., smaller minimum D_p
136   than CPC), additional cases exhibited peak number concentrations in the EIL (10 of 17), with the
137   remaining seven cases showing peak values in the FT. UFCPC number concentrations peaked in
138   the EIL (1400 ± 534 cm^{-3}) and FT (1296 ± 705 cm^{-3}), with the SUB layer again exhibiting the
139   lowest values (530 ± 336 cm^{-3}). PCASP data revealed a different vertical trend than the UFCPC
140   and CPC in that several cases exhibited peak concentrations in the SUB layer (5 of 17), with the
141   most cases exhibiting the highest values in the FT (7 of 17). Average PCASP concentrations
142   were as follows in each layer: 156 ± 65 cm^{-3} (SUB), 224 ± 107 cm^{-3} (EIL), 227 ± 120 cm^{-3} (FT).
143   Relative to the SUB layer, the larger standard deviation of particle concentrations from the three
144   instruments (i.e., PCASP, CPC, UFCPC) in the FT layer for each fight case is most likely owing
145   to weaker vertical mixing, which promotes a non-homogeneous vertical distribution of aerosol in
146   the FT.
147
148   **3.3 Nucleation in the EIL**
149   Discussion in the previous section about differences between the UFCPC and CPC results
150   suggests that new particle formation is a common occurrence in the EIL. Otherwise, it is difficult
151   to explain the enhancements in particle concentrations with D_p between 3 and 10 nm (deduced
152   from the difference between UFCPC and CPC concentrations). Eleven of the 17 cases exhibited
153   their peak ratio of UFCPC:CPC in the EIL, with the remaining six cases split evenly between
154   peak ratios in the SUB and FT layers. Average UFCPC:CPC concentration ratios were as follows
155   in each layer: 1.16 ± 0.04 (SUB), 1.34 ± 0.23 (EIL), 1.18 ± 0.10 (FT). The difference in the
156   means between the EIL and either of the other two layers is statistically significant with 95%
157   confidence based on a two-tailed t test. The difference between the SUB and FT layers is
158   insignificant.
159   To further examine differences in the aerosol size distribution in different vertical layers,
160   Figure 3 shows average number concentrations of particles in three D_p ranges: 3-10 nm (UFCPC-
161   CPC), 10-110 nm (CPC-PCASP), 110-3400 nm (PCASP). Regardless of the D_p range, the SUB
162   layer exhibited the lowest average number concentration relative to the other layers. When
163   considering each vertical layer, the D_p range exhibiting the highest number concentration was
164   10-110 nm. The highest number concentrations of particles with $D_p < 110$ nm were observed in
165   the EIL, FT1, and FT2 layers. Number concentrations with D_p between 3 and 10 nm were
166   highest in EIL (350 ± 220) relative to the other vertical layers with statistically significant
167   differences (at 95% confidence) when compared to the SUB, FT3, and FT4 layers. The highest
168   number concentration of particles with D_p between 10 and 110 nm was observed in the FT2 and
169   FT3 layers, with likely influence from transported emissions of continentally-derived secondarily
170   produced aerosol (e.g., Hersey et al., 2009; Coggon et al., 2014) and growth of new particles
171   from the EIL and lower FT.

172   Factors promoting nucleation include cool and moist air and low particle surface area
173 concentrations (e.g., Kerminen and Wexler, 1996; Pirjola et al., 1998, Clarke et al., 1999, Alam
174 et al., 2003). Figure 4 shows mean values for these parameters in each vertical. Surface area (SA)
175 concentration was quantified separately for particles with D_p between 0.11 and 3.4 µm and for
176 $D_p > 3.4$ µm using PCASP and FSSP probes, respectively. Although not measured, actinic fluxes
177 immediately above cloud top in the EIL are enhanced, which contributes to the likelihood of
178 nucleation owing to increased production of OH by more than a factor of two (Mauldin et al.,
179 1999). Temperature and specific humidity expectedly increase and decrease, respectively, with
180 altitude from the SUB layer up to the FT4 layer. Drier and warmer air in the FT is less favorable
181 for nucleation as compared to the EIL. The highest SA concentrations were expectedly observed
182 in the SUB layer owing to sea spray emissions. The sharp reduction of SA concentration between
183 the SUB and EIL layers is driven by scavenging of aerosol within the cloud. Although average
184 SA concentration, when integrating PCASP and FSSP data together (i.e., D_p between 0.11 – 45
185 µm), decreased with altitude above cloud top, the EIL value (54.7 ± 31.8 µm^2 cm^{-3}) was still
186 much lower relative to the SUB layer (314.8 ± 301.6 µm^2 cm^{-3}), and only 42% higher than that in
187 FT3 (38.4 ± 24.8 µm^2 cm^{-3}), which exhibited the lowest value of any layer. The D_p range driving
188 the changes in SA concentration between each layer was between 3.4 and 45 µm (0.2 – 266.8
189 µm^2 cm^{-3}) since Figure 4 shows much less variability for SA concentration of particles with D_p
190 between 0.11 and 3.4 µm (38.1 – 48.1 µm^2 cm^{-3}).

191   As it could be argued that the SA concentration in the EIL was still not very low in an
192 absolute sense and exceeded values in layers above it, it is important to put the results in the
193 context of other studies. Nucleation events adjacent to marine clouds have been recorded to
194 occur for SA concentrations below 2 µm^2 cm^{-3} in at least one study (Perry and Hobbs, 1995).
195 Clarke et al. (1998) observed nucleation in cloud outflow regions when SA concentrations
196 approached or dropped below ~5-10 µm^2 cm^{-3}. However, recent work shows that increased
197 aerosol loadings suppress nucleation in the boundary layer but enhance it in the lower FT owing
198 to a chain of aerosol-radiation-photochemistry interactions (Quan et al., 2017). Nucleation events
199 in Birmingham, United Kingdom occurred for SA concentrations up to 300 µm^2 cm^{-3}, but with
200 most events below 100 µm^2 cm^{-3} (Alam et al., 2003). Field measurements in Beijing, China
201 suggested that 200 µm^2 cm^{-3} served as a threshold surface area concentration below which
202 nucleation occurred (Cai et al., 2017). The total SA concentration in the EIL between 0.11-45
203 µm in the present study was far lower than that threshold and are below the upper limit of what
204 was observed in Birmingham (Figure 4). With regard to emissions sources that could promote
205 nucleation in the study region, major ones include shipping (e.g., SO_2; Coggon et al., 2012),
206 marine biogenic emissions (e.g., dimethylsulfide, amines; Sorooshian et al., 2009, 2015; Youn et
207 al., 2015), and continental emissions (e.g., NH_3, volatile organic compounds; Braun et al., 2017).

208   The combination of cool and moist air, high actinic solar fluxes, relatively low surface
209 area concentrations as compared to other studies with nucleation events (e.g., Alam et al., 2003;
210 Cai et al., 2017), and several precursor vapor sources builds a case for why nucleation resulted in
211 the highest number concentration of particles with $D_p = 3$-10 nm in the EIL relative to other
212 vertical layers. This result is consistent with previous studies showing that enhanced layers of
213 new particles in FT generally are near cloud top heights (e.g., Clarke et al., 1998, Clarke et al.,
214 1999). The significance of nucleation in the EIL is that these particles impact the transfer of solar
215 radiation owing to both directly scattering light and contributing to the marine atmosphere's
216 cloud condensation nuclei (CCN) budget after growth to sufficiently large sizes.

217

3.4 STBL and FT Influences on the EIL

The vertical profile of aerosol number concentrations in the EIL provides insight into the level of influence between adjacent vertical layers (i.e., STBL and FT). Thirteen of the 17 spirals examined exhibited an increasing trend of PCASP concentration as a function of altitude in the EIL layer (Figure 5). Almost all of the cases (16 of 17) exhibited a positive trend for CPC concentration with altitude (Figure 6). Although not shown, owing to its similarity to CPC data, UFCPC concentrations exhibited a positive trend for 16 cases too. F08 exhibited an overall decrease in CPC concentration with EIL altitude; however, concentrations initially exhibited an increase in the bottom half of the EIL before decreasing. F07 was marked by the highest slope, based on CPC concentrations, and it exhibited the thinnest EIL, which demonstrates the sensitivity of the slopes to EIL thickness.

The slopes of the number concentrations versus altitude in the EIL presumably insight into the relative differences between SUB and lower FT aerosol number concentrations. In other words, a positive slope likely suggests that the lower FT is more polluted as compared to the SUB layer. Figure 7 relates the number concentration slopes in the EIL for the PCASP and CPC as a function of the number concentration difference between the FT1 and the SUB layer. The x-axis is normalized by the EIL depth to account for reduced slopes when EIL depth is high. There is a strong positive relationship for both PCASP and CPC data, supporting the notion that the EIL acts as a layer with properties intermediate to those in the STBL and FT. In other words, the aerosol gradient in the EIL is maintained by the relative difference of aerosol characteristics between STBL and lower FT layers.

An interesting feature of the cases with lower number concentrations in the SUB layer is that they tended to be concurrent with thicker clouds. Figure 8 shows particle concentrations in the SUB layer for the 17 cases divided in two different categories (thin and thick clouds) using the median cloud thickness (333 m) as a dividing threshold value. The number concentration means for D_p between 3-10 nm and 10-110 nm were significantly different (and lower) for thick clouds as compared to thin clouds. This is suggestive of enhanced scavenging (both below cloud and in-cloud scavenging) of particles in comparison to thinner clouds. This is supported by columnar-mean drizzle rates for the thick clouds exceeding those for thin clouds: 3.2 ± 2.2 mm day^{-1} versus 0.4 ± 0.4 mm day^{-1}. A peculiar result is that there was no statistically significant difference in the number concentration for larger particles, which are the ones most likely to activate into cloud droplets and be associated with drizzle drops. Although outside the scope of this study, a potential explanation that will be the subject of forthcoming work is that evaporation of drizzle drops in the SUB layer preserves the concentration of larger particles, while smaller particles are scavenged by drops.

3.5 Cloud-Processed Aerosol in the EIL

While some studies suggest that the EIL air has properties intermediate to the STBL and FT owing to detrainment of air from the STBL (Deardorff, 1980; Gerber et al., 2005), others have not found evidence for detrainment (Faloona et al., 2005; Kurowski et al., 2009). Also, the lowering of cloud top height via mechanisms such as evaporation or drop sedimentation can leave a layer of cloud-processed aerosol in the EIL (Sorooshian et al., 2007; Chen et al., 2012). As those studies were not focused on aerosol size distributions, here we address this issue using PCASP size distribution data. Three case studies (Figure 9) are used to show the range of conditions experienced with reference made to geometric mean diameters of specific PCASP size bins where number concentration modes were observed.

Atmospheric
Chemistry
and Physics
Discussions

264   The N16 case exhibited a unimodal size distribution in the SUB layer with a peak near
265   420 nm. In the FT, there was a clear peak at or below the minimum size limit of the PCASP (110
266   nm). The EIL exhibited an intermediate aerosol size distribution with the peak at the lowest size,
267   similar to the FT, and a peak at 420 nm, similar to the SUB layer. In addition, the number
268   concentration was most enhanced in the EIL in comparison to the SUB and FT layers. The
269   number concentration and shape of the size distribution above 315 nm was identical between the
270   EIL and SUB layers. However, the number concentration below that size was most enhanced in
271   the EIL, suggestive of accumulation of subsiding FT aerosol. Earlier work showed how
272   subsiding FT aerosol can lead to thin layers of enriched organic acid aerosol concentrations
273   above cloud tops in the study region (Sorooshian et al., 2007).
274   The F03-4 case exhibited behavior characteristic of the EIL being mainly influenced by
275   the FT and not the SUB layer. The SUB aerosol size distribution was bimodal with peaks at 182
276   and 223 nm. The FT aerosol exhibited a bimodal distribution but with peaks at smaller sizes,
277   specifically 151 and 182 nm. The EIL showed the same bimodal structure as the FT, with the
278   resemblance closest near the top of the EIL.
279   Finally, the F10-1 case exhibited behavior suggestive of higher influence from the SUB
280   layer as compared to the FT. The SUB aerosol size distribution was bimodal similar to the
281   previous case with peaks at 182 and 223 nm. These same peaks were present in the EIL, and the
282   resemblance to the SUB size distribution was closest at the base of the EIL. The FT aerosol was
283   unimodal with a peak at 182 nm.
284   These three cases illustrate that EIL aerosol size distributions exhibit characteristics of
285   both the STBL and FT aerosol to varying degrees depending on the case examined. The slopes
286   from Figure 5 are consistent with the aerosol size distribution relationships between the SUB,
287   EIL, and FT layers. More specifically, the most significant, and highest slope, was for F03-4,
288   which is the case where the EIL size distribution most clearly resembled that in the FT. Although
289   still positive, the slope from N16 was weaker owing to the influence from both the STBL and
290   FT. Finally, F10-1 exhibited a negative slope, consistent with the EIL size distribution most
291   clearly resembling that in the SUB layer.
292
293   **4. Conclusions**
294   This work examined 17 spiral soundings from research flights off the California coast
295   with a focus on the aerosol characteristics of the EIL relative to the FT above it, and the STBL
296   below it. The main results are as follows:
297
298   •   Regardless of particle size range, the SUB layer exhibits the lowest average number
299   concentrations relative to the EIL and FT. Thicker clouds were coincident with the lowest
300   number concentrations in the SUB layer, especially for D_p between 3 and 110 nm.
301   Conversely, the SUB layer exhibits the highest total aerosol surface area concentrations
302   owing to sea spray emissions, with significantly lower values in the EIL and FT layers.
303   •   The aerosol number concentration data provide evidence of nucleation in the EIL,
304   coincident with factors that promote this mechanism including relatively low aerosol
305   surface area, favorable meteorological conditions (cool and moist air), and high actinic
306   fluxes.

Atmospheric
Chemistry
and Physics
Discussions

307   • Vertical aerosol concentration gradients for PCASP and CPC number concentrations in
308   the EIL are a good predictor as to the relative behavior of the aerosol size distribution
309   between the SUB and FT layers.
310   • Vertically-resolved aerosol size distribution data show that there can be signatures of
311   cloud-processed air in the EIL.

312   The implications of this study are multi-fold with regard to research flight planning and
313 the overall effects of aerosol on climate and clouds. More specifically, the results stress that
314 airborne flights that attempt to characterize aerosol characteristics above stratocumulus clouds
315 require caution in terms of how far above cloud tops flight patterns are conducted owing to
316 differences that exist between the EIL and the FT. Careful attention to where the EIL is relative
317 to the FT is recommended as the latter most clearly will represent aerosol conditions from
318 sources other than those below cloud and the former will have the strongest signature of
319 nucleation. Finally, the EIL often exhibits signatures of cloud-processed aerosol that are
320 important to consider with regard to understanding cloud effects on aerosol.

321 *Data availability:* All data used in this work can be found on the Figshare database (Sorooshian
322 et al., 2017; https://figshare.com/articles/A_Multi-Year_Data_Set_on_Aerosol-Cloud-
323 Precipitation-Meteorology_Interactions_for_Marine_Stratocumulus_Clouds/5099983).
324
325 *Competing interests:* The authors declare that they have no conflict of interest.
326
329
330 **References**
331 Alam, A., Shi, J. P., and Harrison, R. M.: Observations of new particle formation in urban air, J.
332 Geophys. Res.-Atmos., 108, 4093, doi:10.1029/2001jd001417, 2003.
333
334 Braun, R. A., Dadashazar, H., MacDonald, A. B., Aldhaif, A. M., Maudlin, L. C., Crosbie, E.,
335 Aghdam, M. A., Mardi, A. H., and Sorooshian, A.: Impact of Wildfire Emissions on Chloride
336 and Bromide Depletion in Marine Aerosol Particles, Environ. Sci. Technol., 51, 9013-9021,
337 2017.
338
339 Cai, R., Yang, D., Fu, Y., Wang, X., Li, X., Ma, Y., Hao, J., Zheng, J., and Jiang, J.: Aerosol
340 Surface Area Concentration: a Governing Factor for New Particle Formation in Beijing, Atmos.
341 Chem. Phys. Discuss., doi:10.5194/acp-2017-467, in review, 2017.
342
343 Carman, J. K., Rossiter, D. L., Khelif, D., Jonsson, H. H., Faloona, I. C., and Chuang, P. Y.:
344 Observational constraints on entrainment and the entrainment interface layer in stratocumulus,
345 Atmos. Chem. Phys., 12, 11135-11152, doi:10.5194/acp-12-11135-2012, 2012.
346
347 Caughey, S. J., Crease, B. A., and Roach, W. T.: A Field-Study of Nocturnal Stratocumulus .2.
348 Turbulence Structure and Entrainment, Q. J. Roy. Meteor. Soc., 108, 125-144,
349 doi:10.1002/qj.49710845508, 1982.
350

Atmospheric
Chemistry
and Physics
Discussions

351 Chen, Y. C., Christensen, M. W., Xue, L., Sorooshian, A., Stephens, G. L., Rasmussen, R. M.,
352 and Seinfeld, J. H.: Occurrence of lower cloud albedo in ship tracks, Atmos. Chem. Phys., 12,
353 8223-8235, doi:10.5194/acp-12-8223-2012, 2012.

355 Clarke, A. D., Varner, J. L., Eisele, F., Mauldin, R. L., Tanner, D., and Litchy, M.: Particle
356 production in the remote marine atmosphere: Cloud outflow and subsidence during ACE 1, J.
357 Res.-Atmos., 103, 16397-16409, doi:10.1029/97jd02987, 1998.

359 Clarke, A. D., Kapustin, V. N., Eisele, F. L., Weber, R. J., and McMurry, P. H.: Particle
360 production near marine clouds: Sulfuric acid and predictions from classical binary nucleation,
361 Geophys. Res. Lett., 26, 2425-2428, doi:10.1029/1999gl900438, 1999.

363 Coggon, M. M., Sorooshian, A., Wang, Z., Metcalf, A. R., Frossard, A. A., Lin, J. J., Craven, J.
364 S., Nenes, A., Jonsson, H. H., Russell, L. M., Flagan, R. C., and Seinfeld, J. H.: Ship impacts on
365 the marine atmosphere: insights into the contribution of shipping emissions to the properties of
366 marine aerosol and clouds, Atmos. Chem. Phys., 12, 8439-8458, doi:10.5194/acp-12-8439-2012,
367 2012.

369 Coggon, M. M., Sorooshian, A., Wang, Z., Craven, J. S., Metcalf, A. R., Lin, J. J., Nenes, A.,
370 Jonsson, H. H., Flagan, R. C., and Seinfeld, J. H.: Observations of continental biogenic impacts
371 on marine aerosol and clouds off the coast of California, J. Geophys. Res.-Atmos., 119, 6724-
372 6748, doi:10.1002/2013JD021228, 2014.

374 Costantino, L., and Breon, F. M.: Analysis of aerosol-cloud interaction from multi-sensor
375 satellite observations, Geophys. Res. Lett., 37, L11801, doi:10.1029/2009gl041828, 2010.

377 Dadashazar, H., Wang, Z., Crosbie, E., Brunke, M., Zeng, X. B., Jonsson, H., Woods, R. K.,
378 Flagan, R. C., Seinfeld, J. H., and Sorooshian, A.: Relationships between giant sea salt particles
379 and clouds inferred from aircraft physicochemical data, J. Geophys. Res.-Atmos., 122, 3421-
380 3434, doi:10.1002/2016JD026019, 2017.

382 Deardorff, J. W.: Stratocumulus-Capped Mixed Layers Derived from a 3-Dimensional Model,
383 Bound.-Lay. Meteorol., 18, 495-527, doi:10.1007/Bf00119502, 1980.

385 Faloona, I., Lenschow, D. H., Campos, T., Stevens, B., van Zanten, M., Blomquist, B., Thornton,
386 D., Bandy, A., and Gerber, H.: Observations of entrainment in eastern Pacific marine
387 stratocumulus using three conserved scalars, J. Atmos. Sci., 62, 3268-3285,
388 doi:10.1175/Jas3541.1, 2005.

390 Feingold, G., McComiskey, A., Rosenfeld, D., and Sorooshian, A.: On the relationship between
391 cloud contact time and precipitation susceptibility to aerosol, J. Geophys. Res.-Atmos., 118,
392 10544-10554, doi:10.1002/jgrd.50819, 2013.

394 Gerber, H., Arends, B. G., and Ackerman, A. S.: New microphysics sensor for aircraft use,
395 Atmos. Res., 31, 235-252, doi:10.1016/0169-8095(94)90001-9, 1994.

396

Atmospheric
Chemistry
and Physics
Discussions

397 Gerber, H., Frick, G., Malinowski, S. P., Brenguier, J. L., and Burnet, F.: Holes and entrainment
398 in stratocumulus, J. Atmos. Sci., 62, 443-459, doi:10.1175/Jas-3399.1, 2005.
399
400 Gerber, H., Frick, G., Malinowski, S. P., Jonsson, H., Khelif, D., and Krueger, S. K.:
401 Entrainment rates and microphysics in POST stratocumulus, J. Geophys. Res.-Atmos., 118,
402 12094-12109, doi:10.1002/jgrd.50878, 2013.
403
404 Haman, K. E., Malinowski, S. P., Kurowski, M. J., Gerber, H., and Brenguier, J. L.: Small scale
405 mixing processes at the top of a marine stratocumulus - a case study, Q. J. Roy. Meteor. Soc.,
406 133, 213-226, doi:10.1002/qj.5, 2007.
407
408 Hegg, D. A., Covert, D. S., Jonsson, H., and Covert, P. A.: Determination of the transmission
409 efficiency of an aircraft aerosol inlet, Aerosol Sci. Tech., 39, 966-971,
410 doi:10.1080/02786820500377814, 2005.
411
412 Hersey, S. P., Sorooshian, A., Murphy, S. M., Flagan, R. C., and Seinfeld, J. H.: Aerosol
413 hygroscopicity in the marine atmosphere: a closure study using high-time-resolution, multiple-
414 RH DASH-SP and size-resolved C-ToF-AMS data, Atmos. Chem. Phys., 9, 2543-2554,
415 doi:10.5194/acp-9-2543-2009, 2009.
416
417 Katoshevski, D., Nenes, A., and Seinfeld, J. H.: A study of processes that govern the
418 maintenance of aerosols in the marine boundary layer, J. Aerosol. Sci., 30, 503-532,
419 doi:10.1016/S0021-8502(98)00740-X, 1999.
420
421 Katzwinkel, J., Siebert, H., and Shaw, R. A.: Observation of a Self-Limiting, Shear-Induced
422 Turbulent Inversion Layer Above Marine Stratocumulus, Bound.-Lay. Meteorol., 145, 131-143,
423 doi:10.1007/s10546-011-9683-4, 2012.
424
425 Kerminen, V. M., and Wexler, A. S.: The occurrence of sulfuric acid-water nucleation in plumes:
426 Urban environment, Tellus B, 48, 65-82, doi:10.1034/j.1600-0889.1996.00007.x, 1996.
427
428 Kurowski, M. J., Malinowski, S. P., and Grabowski, W. W.: A numerical investigation of
429 entrainment and transport within a stratocumulus-topped boundary layer, Q. J. Roy. Meteor.
430 Soc., 135, 77-92, doi:10.1002/qj.354, 2009.
431
432 Lenschow, D. H., Zhou, M. Y., Zeng, X. B., Chen, L. S., and Xu, X. D.: Measurements of fine-
433 scale structure at the top of Marine Stratocumulus, Bound.-Lay. Meteorol., 97, 331-357, doi:
434 10.1023/A:1002780019748, 2000.
435
436 Malinowski, S. P., Gerber, H., Jen-La Plante, I., Kopec, M. K., Kumala, W., Nurowska, K.,
437 Chuang, P. Y., Khelif, D., and Haman, K. E.: Physics of Stratocumulus Top (POST): turbulent
438 mixing across capping inversion, Atmos. Chem. Phys., 13, 12171-12186, doi:10.5194/acp-13-
439 12171-2013, 2013.
440
441 Maudlin, L. C., Wang, Z., Jonsson, H. H., and Sorooshian, A.: Impact of wildfires on size-
442 resolved aerosol composition at a coastal California site, Atmos. Environ., 119, 59-68, 2015.

443
444   Mauldin, R. L., Tanner, D. J., Heath, J. A., Huebert, B. J., and Eisele, F. L.: Observations of
445   H_2SO_4 and MSA during PEM-Tropics-A, J. Geophys. Res.-Atmos., 104, 5801-5816,
446   doi:10.1029/98jd02612, 1999.
447
448   Moeng, C. H., Stevens, B., and Sullivan, P. P.: Where is the interface of the stratocumulus-
449   topped PBL?, J. Atmos. Sci., 62, 2626-2631, doi:10.1175/Jas3470.1, 2005.
450
451   Nicholls, S., and Turton, J. D.: An Observational Study of the Structure of Stratiform Cloud
452   Sheets .2. Entrainment, Q. J. Roy. Meteor. Soc., 112, 461-480, doi:10.1002/qj.49711247210,
453   1986.
454
455   Perry, K. D., and Hobbs, P. V.: Further Evidence for Particle Nucleation in Clean-Air Adjacent
456   to Marine Cumulus Clouds, J. Geophys. Res.-Atmos., 100, 18929-18929,
457   doi: 10.1029/94JD01926, 1995.
458
459   Pirjola, L., Kulmala, M., Wilck, M., Bischoff, A., Stratmann, F., and Otto, E.: Formation of
460   sulphuric acid aerosols and cloud condensation nuclei: An expression for significant nucleation
461   and model comparison, J. Aerosol. Sci., 30, 1079-1094, doi:10.1016/S0021-8502(98)00776-9,
462   1999.
463
464   Prabhakar, G., Ervens, B., Wang, Z., Maudlin, L. C., Coggon, M. M., Jonsson, H. H., Seinfeld, J.
465   H., and Sorooshian, A.: Sources of nitrate in stratocumulus cloud water: Airborne measurements
466   during the 2011 E-PEACE and 2013 NiCE studies, Atmos. Environ., 97, 166-173, 2014.
467
468   Quan, J. N., Liu, Y. A., Liu, Q., Jia, X. C., Li, X., Gao, Y., Ding, D. P., Li, J., and Wang, Z. F.:
469   Anthropogenic pollution elevates the peak height of new particle formation from planetary
470   boundary layer to lower free troposphere, Geophys. Res. Lett., 44, 7537-7543,
471   doi: 10.1002/2017GL074553, 2017.
472
473   Radke, L. F., Hobbs, P. V., and Eltgroth, M. W.: Scavenging of Aerosol-Particles by
474   Precipitation, J. Appl. Meteorol., 19, 715-722, doi:10.1175/1520-
475   0450(1980)019<0715:Soapbp>2.0.Co;2, 1980.
476
477   Sorooshian, A., Lu, M. L., Brechtel, F. J., Jonsson, H., Feingold, G., Flagan, R. C., and Seinfeld,
478   J. H.: On the source of organic acid aerosol layers above clouds, Environ. Sci. Technol., 41,
479   4647-4654, doi:10.1021/es0630442, 2007.
480
481   Sorooshian, A., Padro, L. T., Nenes, A., Feingold, G., McComiskey, A., Hersey, S. P., Gates, H.,
482   Jonsson, H. H., Miller, S. D., Stephens, G. L., Flagan, R. C., and Seinfeld, J. H.: On the link
483   between ocean biota emissions, aerosol, and maritime clouds: Airborne, ground, and satellite
484   measurements off the coast of California, Global Biogeochem. Cy., 23,
485   doi:10.1029/2009GB003464, 2009.
486
487   Sorooshian, A., Crosbie, E., Maudlin, L. C., Youn, J. S., Wang, Z., Shingler, T., Ortega, A. M.,
488   Hersey, S., and Woods, R. K.: Surface and airborne measurements of organosulfur and

Atmospheric
Chemistry
and Physics
Discussions

489 methanesulfonate over the western United States and coastal areas, J. Geophys. Res.-Atmos.,
490 120, 8535-8548, 2015.

492 Sorooshian, A., et al.: A Multi-Year Data Set on Aerosol-Cloud-Precipitation-Meteorology
493 Interactions for Marine Stratocumulus Clouds, Figshare, doi:10.6084/m9.figshare.5099983.v3,
494 2017.

496 Wang, Q., and Albrecht, B. A.: Observations of Cloud-Top Entrainment in Marine
497 Stratocumulus Clouds, J. Atmos. Sci., 51, 1530-1547, doi:10.1175/1520-
498 0469(1994)051<1530:Ooctei>2.0.Co;2, 1994.

500 Wang, S. P., Golaz, J. C., and Wang, Q.: Effect of intense wind shear across the inversion on
501 stratocumulus clouds, Geophys. Res. Lett., 35, L15814, doi:10.1029/2008gl033865, 2008.

503 Wang, Z., Sorooshian, A., Prabhakar, G., Coggon, M. M., and Jonsson, H. H.: Impact of
504 emissions from shipping, land, and the ocean on stratocumulus cloud water elemental
505 composition during the 2011 E-PEACE field campaign, Atmos. Environ., 89, 570-580,
506 doi:10.1016/j.atmosenv.2014.01.020, 2014.

517 Wang, Z., Ramirez, M. M., Dadashazar, H., MacDonald, A. B., Crosbie, E., Bates, K. H.,
518 Coggon, M. M., Craven, J. S., Lynch, P., Campbell, J. R., Aghdam, M. A., Woods, R. K.,
519 Jonsson, H., Flagan, R. C., Seinfeld, J. H., and Sorooshian, A.: Contrasting cloud composition
520 between coupled and decoupled marine boundary layer clouds, J. Geophys. Res.-Atmos., 121,
521 11679-11691, doi:10.1002/2016JD025695, 2016.

523 Warren, S., Hahn, C. J., London, J., Chervin, R. M., and Jenne, R. L. (1986), Global distribution
524 of total cloud cover and cloud types over land, NCAR Tech. Note NCAR/TN-273+STR, 29 pp. +
525 200 maps, Natl. Cent. Atmos. Res., Boulder, Colo.

527 Wood, R.: Stratocumulus Clouds, Mon Weather Rev, 140, 2373-2423, 10.1175/Mwr-D-11-
528 00121.1, 2012.

530 Yamaguchi, T., Feingold, G., Kazil, J., and McComiskey, A.: Stratocumulus to cumulus
531 transition in the presence of elevated smoke layers, Geophys. Res. Lett., 42, 10478-10485,
532 doi:10.1002/2015GL066544, 2015.

534 Youn, J. S., Crosbie, E., Maudlin, L. C., Wang, Z., and Sorooshian, A.: Dimethylamine as a
535 major alkyl amine species in particles and cloud water: Observations in semi-arid and coastal
536 regions, Atmos. Environ., 122, 250-258, doi:10.1016/j.atmosenv.2015.09.061, 2015.

Atmospheric
Chemistry
and Physics
Discussions

538 **Table 1:** Summary of EIL thickness (Thickness (base altitude, top altitude)), and particle concentrations (average (relative
539 standard deviation as a percentage)) for the sub-cloud layer (SUB), the entrainment interface layer (EIL), and the free
540 troposphere (FT). The cases are labeled with the campaign (F = FASE, N = NiCE), research flight number, and case number
541 (only for flights with more than one spiral) from that flight (i.e., 'F12-2' is the second spiral sounding case from FASE
542 Research Flight 12).
543
544

| Case	EIL Thickness (m)	PCASP (cm^{-3})			CPC (cm^{-3})			UFCPC (cm^{-3})		
		SUB	EIL	FT	SUB	EIL	FT	SUB	EIL	FT
F03-1	22 (692,714)	129 (20)	273 (15)	245 (47)	186 (10)	1337 (16)	1106 (38)	232 (15)	1542 (24)	1382 (39)
F03-2	19 (729,748)	192 (15)	428 (11)	442 (54)	300 (3)	1259 (29)	1499 (40)	352 (8)	1767 (22)	1843 (42)
F03-3	27 (698,725)	199 (9)	353 (32)	258 (99)	272 (2)	868 (62)	919 (71)	324 (9)	1437 (49)	1254 (73)
F03-4	32 (700,732)	145 (17)	326 (36)	266 (70)	185 (5)	1553 (20)	1023 (63)	210 (67)	1950 (30)	1539 (64)
F07	10 (513,523)	268 (8)	245 (15)	275 (43)	861 (1)	1765 (50)	2043 (20)	991 (7)	2615 (48)	2407 (26)
F08	39 (375,414)	136 (11)	109 (11)	67 (49)	1010 (10)	1043 (8)	698 (23)	1207 (20)	1220 (14)	799 (27)
F09-1	23 (412,435)	206 (7)	170 (8)	189 (21)	688 (1)	1062 (15)	1268 (19)	837 (11)	1296 (18)	1444 (23)
F09-2	59 (403,462)	253 (7)	205 (11)	131 (27)	999 (2)	1353 (26)	841 (28)	1169 (12)	1619 (25)	942 (30)
F10-1	31 (637,668)	213 (17)	206 (17)	114 (18)	355 (5)	887 (27)	477 (26)	422 (8)	1054 (22)	543 (28)
F10-2	28 (600,628)	166 (11)	253 (29)	138 (87)	276 (2)	833 (47)	455 (77)	315 (11)	1137 (41)	494 (80)
F11	70 (707,777)	50 (26)	171 (92)	430 (25)	194 (8)	654 (74)	1212 (27)	222 (10)	806 (68)	1337 (30)
F12-1	28 (500,528)	181 (9)	255 (12)	374 (32)	661 (3)	804 (5)	782 (10)	789 (9)	921 (8)	904 (14)
F12-2	15 (444,459)	77 (12)	54 (13)	35 (40)	357 (11)	334 (3)	433 (82)	402 (17)	376 (5)	509 (122)
F14-1	24 (614,638)	57 (30)	112 (39)	338 (21)	350 (4)	1522 (31)	2281 (5)	398 (8)	2011 (30)	2668 (6)
F14-2	43 (525,568)	91 (15)	87 (52)	166 (12)	459 (17)	1308 (55)	2402 (1)	490 (16)	1707 (49)	2660 (5)
F16	33 (443,476)	103 (12)	163 (43)	236 (6)	185 (5)	601 (69)	1222 (3)	209 (12)	907 (52)	1403 (6)
N16	15 (649,664)	183 (15)	391 (12)	155 (47)	385 (3)	703 (74)	657 (43)	433 (6)	1441 (42)	735 (38)

545
546

547

14
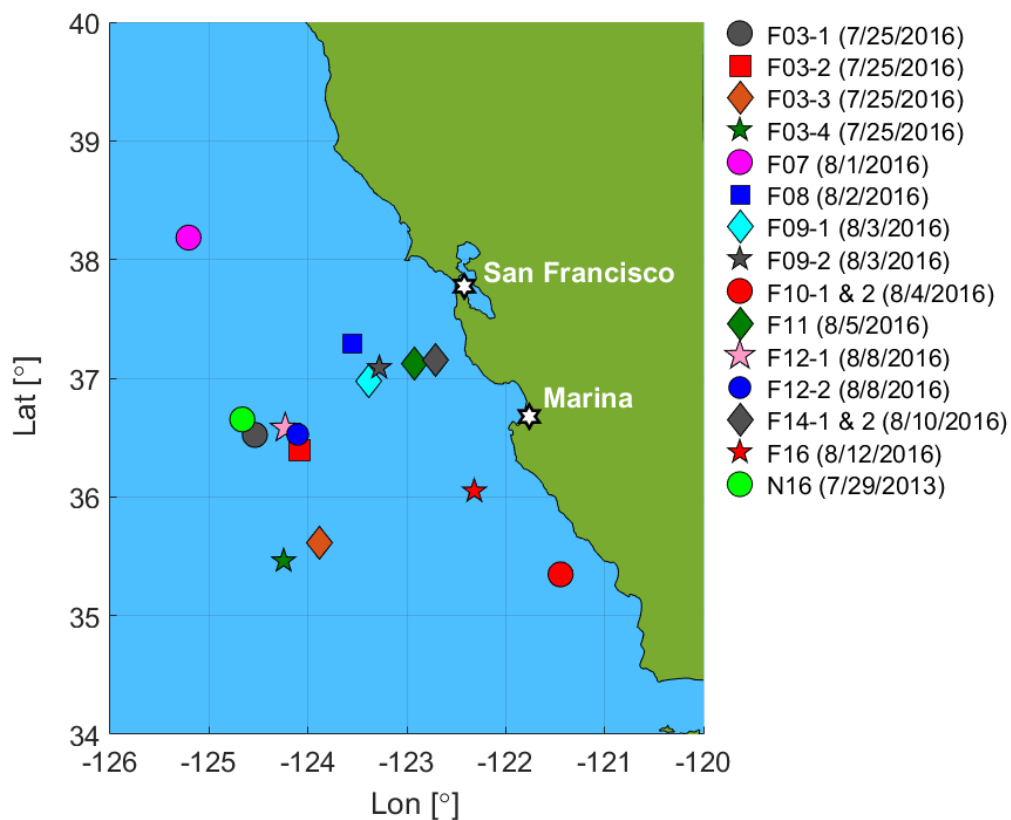
548

549

550 **Figure 1: Spatial map of spiral soundings examined in this study from the NiCE (2013) and**
551 **FASE (2016) field campaigns. The cases are labeled with the campaign (F = FASE, N =**
552 **NiCE), research flight number, and case number (only for flights with more than one**
553 **spiral) from that flight (i.e., 'F12-2' is the second spiral sounding case from FASE Research**
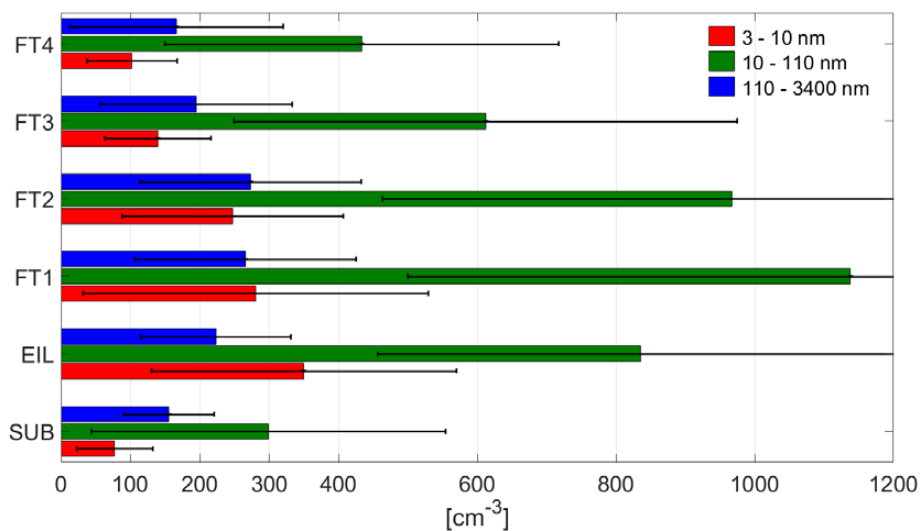554 **Flight 12).**

555

556
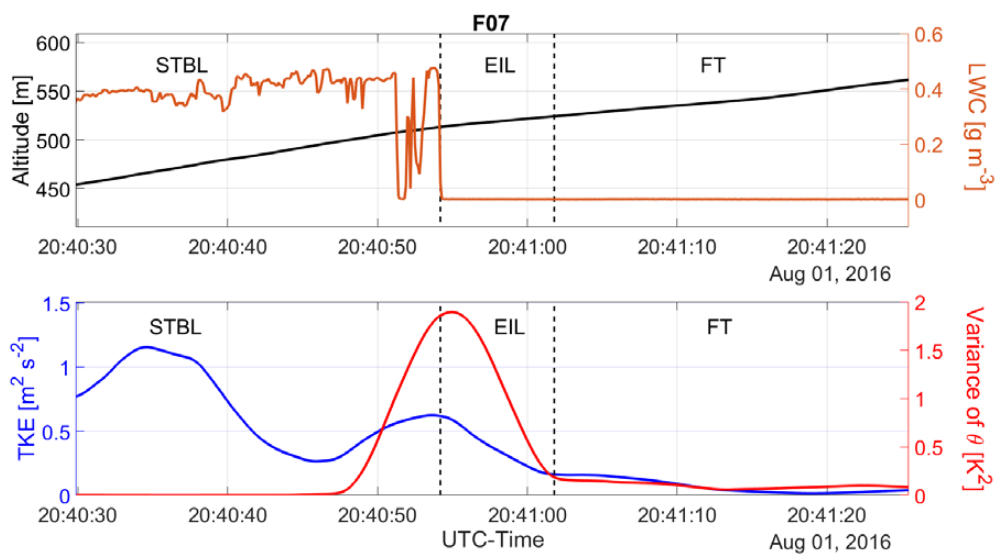
Figure 2: F07 on 1 August 2016 showing how thermodynamic and dynamic criteria were applied to define the vertical bounds of the EIL, which separates the STBL from the FT. This subset of data is obtained from an upward spiral sounding.

561

Figure 3: Particle concentrations in different diameter ranges (3-10 nm, 10-110 nm, 110-3400 nm) for SUB, EIL, and FT vertical layers. The FT is divided into four layers based on 100 m increments above the EIL top. Whiskers represent one standard deviation.

568

569
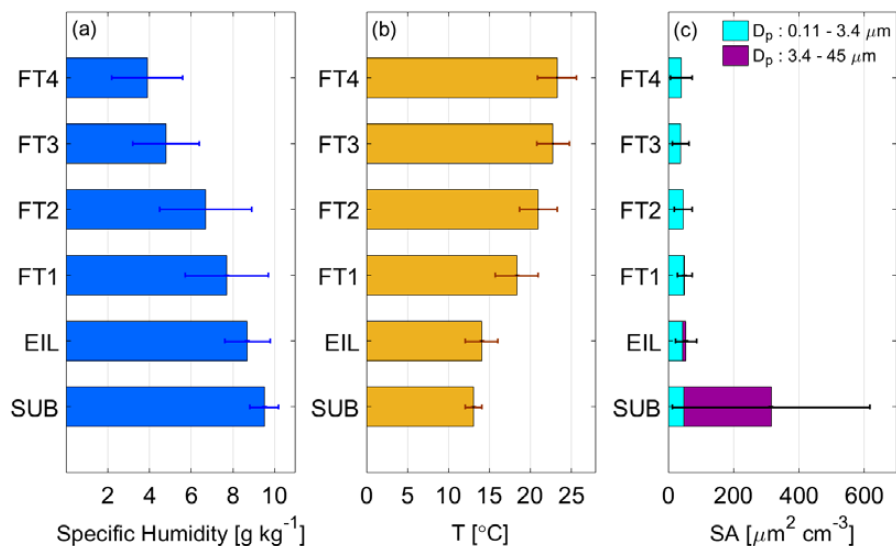
Figure 4: (a) Specific humidity, (b) temperature, and (c) particle surface area (SA) concentrations for the SUB, EIL, and FT layers. The FT is divided into four layers based on 100 m increments above the EIL top. Particle SA concentrations are shown separately for the following diameter ranges: 0.11 - 3.4 μm, 3.4 - 45 μm. Whiskers represent one standard deviation.
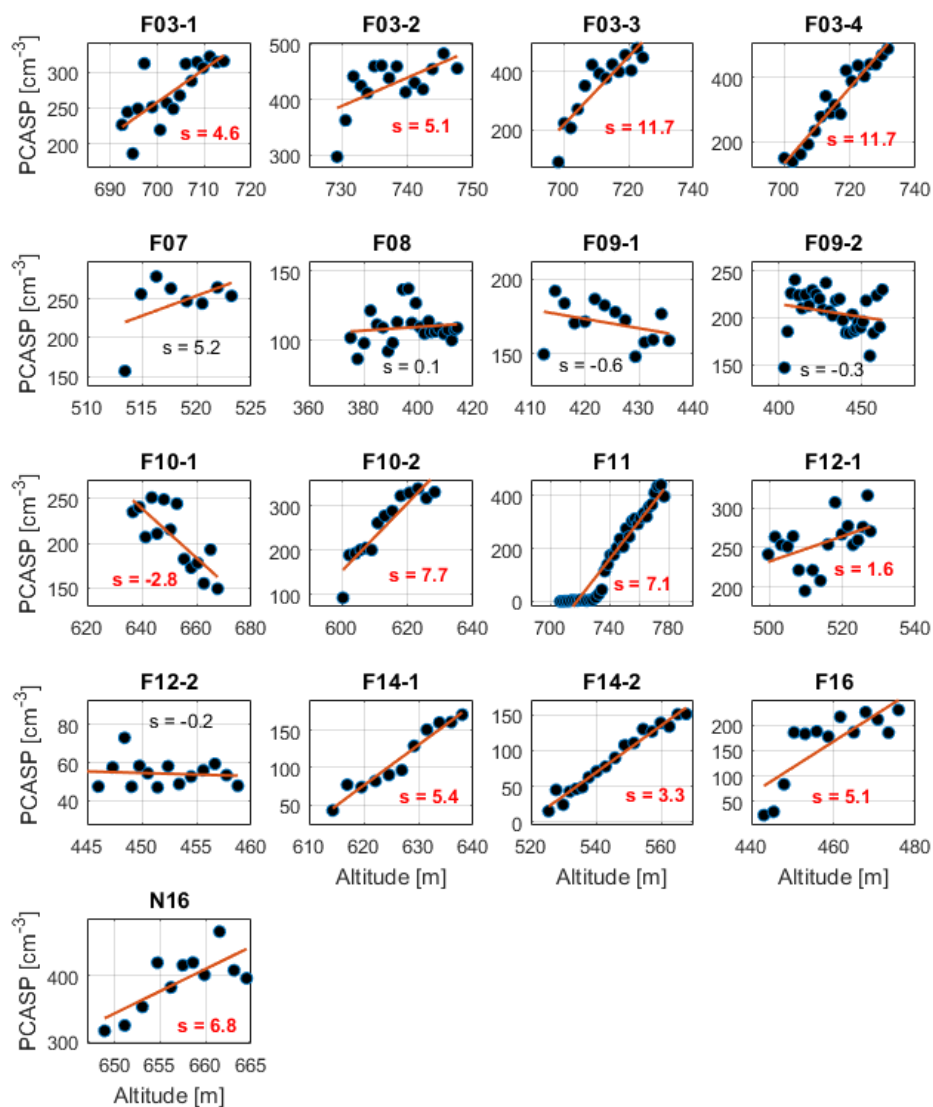
Figure 5: PCASP concentration as a function of altitude in the EIL. Linear fits and slopes (s, units of cm^{-3} m^{-1}) are shown in each panel. Slopes in red font correspond to statistically significant correlations at 95% based on a two-tailed t test.
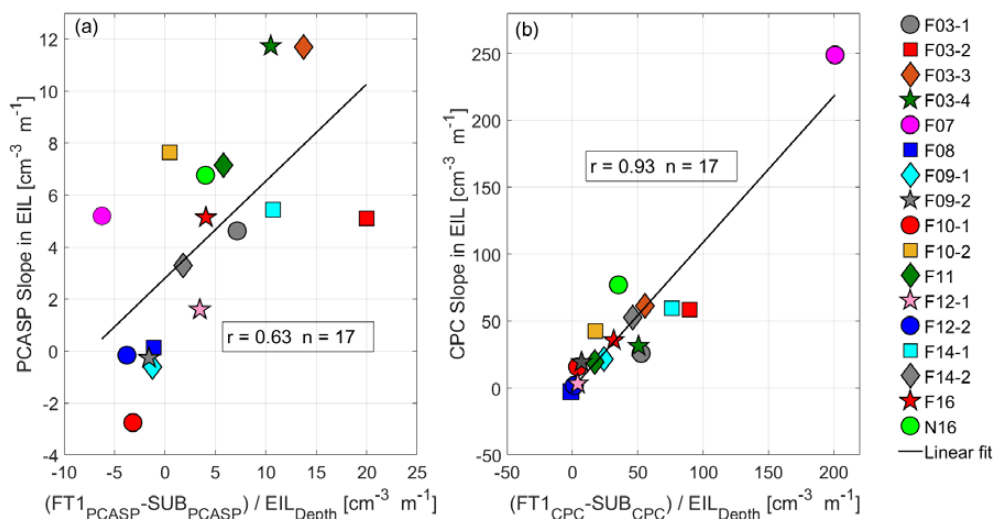
Atmospheric
Chemistry
and Physics
Discussions
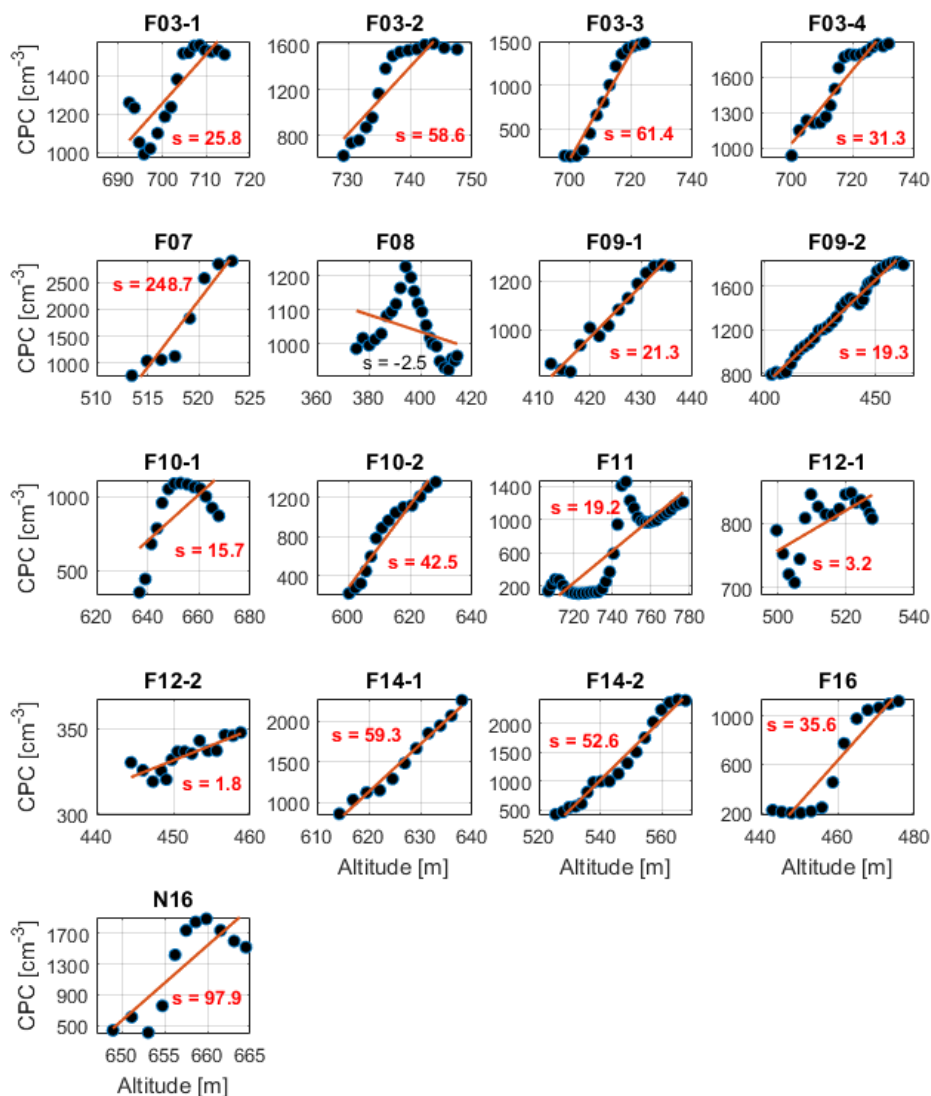
Figure 6: CPC concentration as a function of altitude in EIL. Linear fits and slopes (s, units of cm^{-3} m^{-1}) are shown in each panel. Slopes in red font correspond to statistically significant correlations at 95% based on a two-tailed t test.

Atmospheric
Chemistry
and Physics
Discussions

Open Access

584

585
586
587 **Figure 7: Relationship between the slope of particle concentration gradients in EIL and**
588 **concentration differences between the FT1 and SUB layers. Results are shown for the (a)**
589 **PCASP and (b) CPC. The x-axis is normalized by the EIL depth to account for reduced**
590 **slopes when the EIL is deeper.**
591

Atmospheric
Chemistry
and Physics
Discussions

Open Access
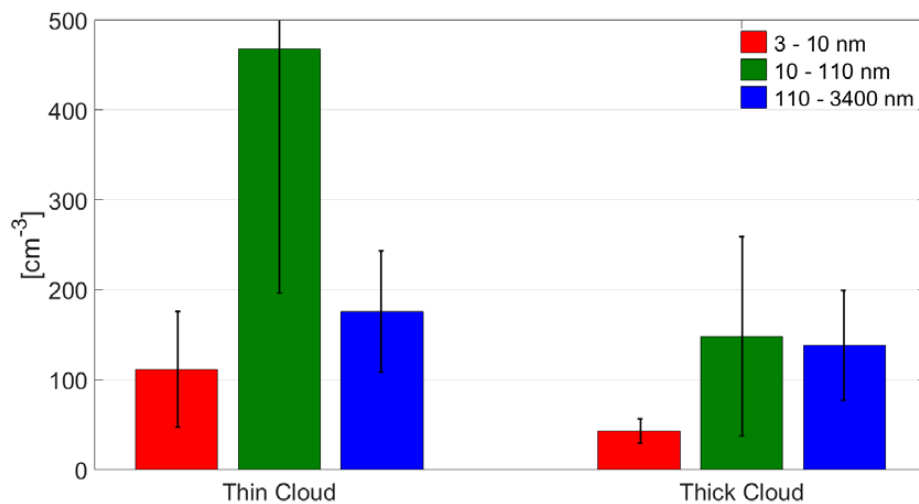
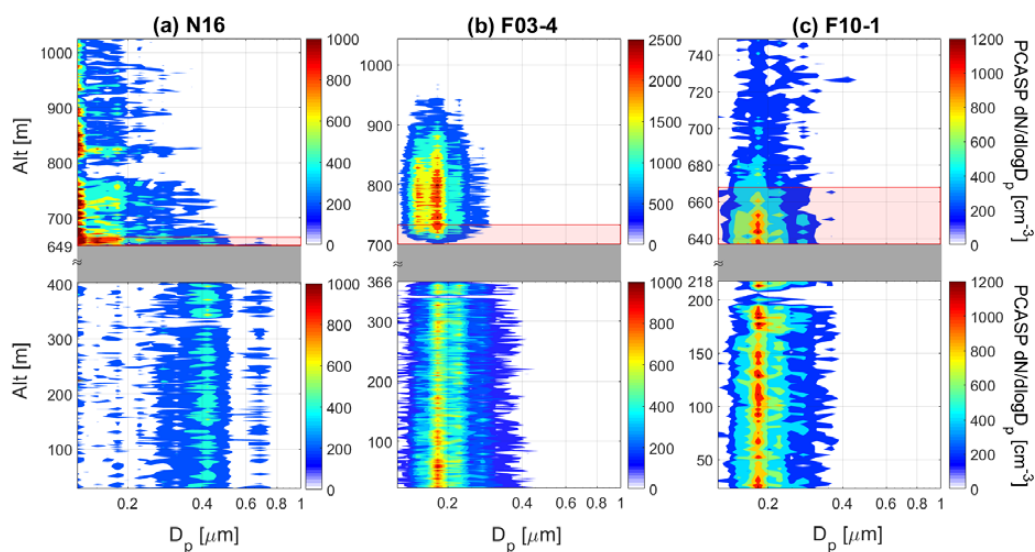**Figure 8: Particle concentrations in different diameter ranges (3-10 nm, 10-110 nm, 110-3400 nm) in the sub-cloud (SUB) layer for thin (thickness < 333 m) and thick (thickness ≥ 333 m) clouds. Whiskers represent one standard deviation.**

596
597

598
599 **Figure 9: Vertically-resolved aerosol size distributions during spiral soundings on (a) N16,**
600 **(b) F03-4, and (c) F10-1. The EIL and cloud layers are shaded in red and grey, respectively.**
601